J. Fluid Mech. (1984), *vol.* 138, *pp.* 273–295
Printed in Great Britain

Sound generated by instability waves of supersonic flows. Part 2. Axisymmetric jets

By CHRISTOPHER K. W. TAM AND DALE E. BURTON
Department of Mathematics, Florida State University, Tallahassee, Florida 32306

(Received 20 December 1982)

A solution describing the spatial evolution of small-amplitude instability waves and their associated sound field of axisymmetric supersonic jets is found using the method of matched asymptotic expansions (see Part 1, Tam & Burton 1984). The inherent axisymmetry of the problem allows the instability waves to be decomposed into azimuthal wave modes. In addition, it is found that because of the cylindrical geometry of the problem the gauge functions of the inner expansion, unlike the case of two-dimensional mixing layers, are no longer just powers of ϵ. Instead they contain logarithmic terms. To test the validity of the theory, numerical results of the solution are compared with the experimental measurements of Troutt (1978) and Troutt & McLaughlin (1982). Two series of comparisons at Strouhal numbers 0.2 and 0.4 for a Mach-number 2.1 cold supersonic jet are made. The data compared include hot-wire measurements of the axial distribution of root-mean-squared jet centreline mass-velocity fluctuations and radial and axial distributions of near-field pressure-level contours measured by microphones. The former is used to test the accuracy of the inner (or instability-wave) solution. The latter is used to verify the correctness of the outer solution. Very favourable overall agreements between the calculated results and the experimental measurements are found. These very favourable agreements strongly suggest that the method of solution developed in Part 1 paper is indeed valid. Furthermore, they also offer concrete support to the proposition made previously by a number of investigators that instability waves are important noise sources in supersonic jets.

1. Introduction

In the companion paper (Part 1, Tam & Burton 1984) the problem of sound generation by instability waves of supersonic compressible two-dimensional mixing layers is solved by the method of matched asymptotic expansions. The purpose of this study is to test the validity of the theory by applying it to an axisymmetric supersonic jet and comparing the calculated results with experimental measurements. The experimental measurements are to be taken from the recent investigation of Troutt (1978) and Troutt & McLaughlin (1982). As far as is known, these investigators provided the only set of good-quality data showing the direct generation of sound by large-scale instability waves of a jet at moderately high Reynolds numbers. (High-frequency sound generated by small-scale instability waves in the initial mixing layer of a supersonic jet was first considered and proven theoretically and experimentally by Tam (1971) and Chan & Westley (1973).) Two series of their hot-wire and microphone data involving instability waves gently excited by a glow discharge mounted flush near the nozzle exit of a 2.1 Mach-number jet at Strouhal numbers 0.2 and 0.4 will be used. Detailed comparison of the calculated and measured spatial

distribution of the excited instability wave amplitudes along the centreline of the jet as well as the sound-wave pressure amplitudes in the near field immediately outside the jet will be made. The former may be considered as a test of the accuracy of the inner solution or the instability-wave solution. Whereas the latter could be regarded as a verification of the validity of the outer solution. In the study of Troutt (1978) and Troutt & McLaughlin (1982) the experiment was, unfortunately, carried out in an anechoic room of somewhat limited size. Because of this, only flow-field and near-pressure-field data were acquired with sufficient precision. Accurate far-field noise data, which can only be obtained by microphones located at distances, at least, 150 to 200 jet diameters away from the jet nozzle exit, are not available for comparison with calculation.

In applying the theory of Part 1 to the case of a round jet, the axisymmetric geometry of the problem leads immediately to solutions involving Hankel functions of complex order. Thus some of the terms of the asymptotic expansions may, on a first glance, appear to be very complicated. However, when the procedure developed in Part 1 is followed, the whole analysis can be carried out with no special difficulty. Only the algebra becomes rather messy and somewhat complicated. One major difference between the axisymmetric jet and the two-dimensional mixing-layer problems, aside from the appearance of very involved special functions, is that the asymptotic expansions now consist of logarithmic terms. The lowest order of these terms has the form $\epsilon \ln \epsilon$, which is familiar in many singular perturbation problems. As a result, the gauge functions of the inner expansion can no longer be taken as powers of ϵ, but must be determined as a part of the matching process (see e.g. Van Dyke 1975).

Before proceeding to compare the present theory of sound generation by linear instability waves and experiments, one question of considerable importance which one must ascertain is how important are nonlinear effects. In the experiment of Troutt (1978) and Troutt & McLaughlin (1982) an effort was made to keep the excitation level introduced by their glow discharge near the jet nozzle exit very small. This in effect minimizes the contribution of flow nonlinearities. In the present problem, nonlinearities may be divided into nonlinear interaction between the excited instability waves and the mean flow, and the nonlinear self-interaction of the instability waves. The former leads to a change in the mean-flow distribution (or profile) due to the presence of the waves. This in turn modifies the propagation characteristics of the instability waves. Nonlinear effects of this kind will be taken into account in the present study by using the measured mean-flow profiles in the presence of the excited instability waves as an input to the calculation. In other words, the instability waves are linear perturbations superimposed on the forced mean flow. The effects of nonlinear self-interaction of the instability waves will be neglected in this paper. One important consequence of such self-interaction is the generation of harmonics. Experimental measurements by Troutt and Troutt & McLaughlin indicate that harmonics are indeed present in the flow near the nozzle exit. It is possible, however, that these harmonics are generated by the nonlinear excitation process rather than by the nonlinear self-interaction of the excited instability wave. This belief is based on the observation that the amplitudes of these harmonics decrease rapidly to an insignificant value over a short distance downstream of the nozzle exit while the excited fundamental wave is still growing in amplitude spatially. In any case, in the neighbourhood where the excited instability wave attains its maximum amplitude, and therefore is most effective in sound generation, the relative amplitudes of the harmonics seem to be very small. Hence as a first approximation the nonlinear effect of self-interaction will be completely ignored in the calculation. In connection with

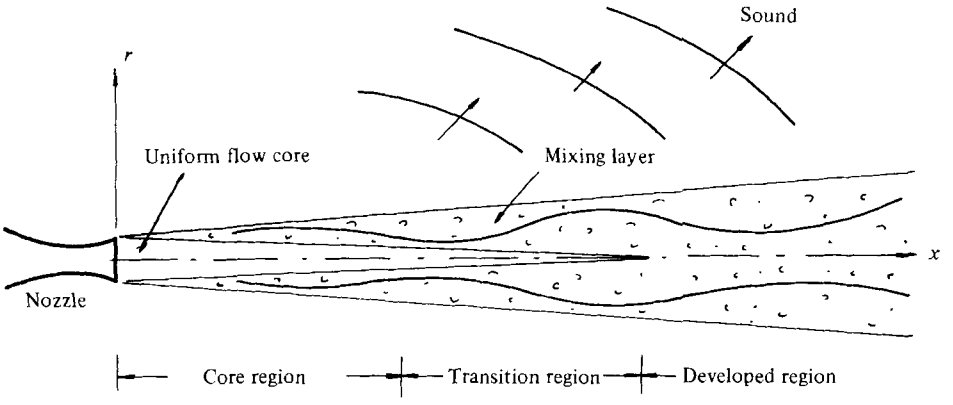

FIGURE 1. Instability waves and their sound field of an axisymmetric jet.

the question of nonlinear effects it is worth while to point out that the spatial growth, peaking and decay of the amplitude of an instability wave in the flow direction of a jet are controlled primarily by the local linear properties of the wave. These linear propagation characteristics of the waves are determined by the local mean-flow profile. The spatial change of the mean-flow profile if a jet in the downstream direction is the main factor that determines the spatial distribution of the wave amplitude. The fact that the wave only attains a finite amplitude is not due to a nonlinear saturation effect as in the case of Taylor vortices or Bénard cells. For waves of moderate amplitudes, nonlinearity is of only secondary importance in controlling their growth or decay in jets and mixing layers.

2. The physical problem and the inner solution

We consider the spatial evolution of a small-amplitude instability wave of angular frequency ω of an axisymmetric supersonic jet as shown in figure 1. The instability wave and its associated acoustic field are governed by the linearized equations of motion for an inviscid compressible fluid. In the following, dimensionless variables will be used. The length, velocity, time, density and pressure scales are R_j (the jet radius at the nozzle exit), u_j (the jet exit velocity), R_j/u_j, ρ_j (the jet exit density) and $\rho_j u_j^2$ respectively. The mean velocity of the jet is assumed to be known. In the numerical calculation the measured velocity profiles are used. With respect to a cylindrical coordinate system (x, r, ϕ) centred at the nozzle exit and the corresponding velocity components (u, v, w) as shown in figure 1, the mean flow which changes slowly in the flow direction may be represented analytically in the form

$$\bar{\boldsymbol{u}} = (\bar{u}(r, s), \epsilon\bar{v}_1(r, s,), 0), \tag{2.1a}$$

where

$$\bar{u} = 0, \quad \epsilon\bar{v}_1 = \frac{\epsilon\bar{v}_\infty}{r} \quad (r \geqslant r_m(s)). \tag{2.1b, c}$$

In (2.1) ϵ is the rate of spread of the mixing layer in the initial part of the jet. Numerically ϵ is less than 0.1. It will be considered as the small parameter of the problem. $s = \epsilon x$ is the slow variable in the downstream direction. The mean radial velocity component is usually, at least, an order of magnitude smaller than the axial component. As a result, it has seldom been measured, and was not measured in the study of Troutt (1978) and Troutt & McLaughlin (1982). Here it will be calculated

by integrating the mean continuity equation. The numerical value of $\bar{v}_\infty$ in (2.1c) is quite small and is of no great significance to the overall problem. For simplicity it will be regarded as a constant. The mean pressure of the jet, as in the case of two-dimensional mixing layers, is nearly constant and is equal to the ambient pressure. The condition of constancy of total temperature will be used to calculate the mean density $\bar{\rho}$. This is a good approximation for cold jets. A further approximation by assuming the mean static temperature and hence the density to be constant in the mean continuity equation of the jet used in the experiment of Troutt and Troutt & McLaughlin has been found numerically to have negligible effect on the computed instability waves.

Since the jet flow is axisymmetric, the instability waves can be Fourier-decomposed into azimuthal modes. All the physical variables can therefore be represented in the form $p'(x, r, \phi, t) = \mathrm{Re}\,[p(r, x)\exp(in\phi - i\omega t)]$ etc., where n is an integer and Re = the real part of. On factoring out the exponential dependence on ϕ and t the governing equations for the spatial part of the solution written in cylindrical coordinates are

$$\left.\begin{aligned} -i\omega v + \bar{v}\frac{\partial v}{\partial r} + v\frac{\partial \bar{v}}{\partial r} + \bar{u}\frac{\partial v}{\partial x} + u\frac{\partial \bar{v}}{\partial x} &= -\frac{1}{\bar{\rho}}\frac{\partial p}{\partial r}, \\ -i\omega w + \bar{v}\frac{\partial w}{\partial r} + \frac{\bar{v}w}{r} + \bar{u}\frac{\partial w}{\partial x} &= -\frac{in}{\bar{\rho}r}p, \\ -i\omega u + \bar{v}\frac{\partial u}{\partial r} + v\frac{\partial \bar{u}}{\partial r} + u\frac{\partial \bar{u}}{\partial x} + \bar{u}\frac{\partial u}{\partial x} &= -\frac{1}{\bar{\rho}}\frac{\partial p}{\partial x}, \\ -i\omega p + \bar{v}\frac{\partial p}{\partial r} + \bar{u}\frac{\partial p}{\partial r} + \frac{1}{M^2}\left(\frac{1}{r}\frac{\partial vr}{\partial r} + \frac{in}{r}w + \frac{\partial u}{\partial x}\right) &= 0. \end{aligned}\right\} \tag{2.2}$$

To construct an inner solution of (2.2) we will follow the choice of inner variables as discussed in Part 1. The appropriate variables are (r, s), where $s = \epsilon x$. The inner solution represents a wave propagating in an inhomogeneous medium formed by the mean flow of the jet. Such a wave may be written in the form (see Whitham 1974, chapter 11)

$$\begin{bmatrix} u(x,r) \\ v(x,r) \\ w(x,r) \\ p(x,r) \end{bmatrix} = \sum_{m=0}^{\infty} \delta_m(\epsilon) \begin{bmatrix} \hat{u}_m(r,s) \\ \hat{v}_m(r,s) \\ \hat{w}_m(r,s) \\ \hat{p}_m(r,s) \end{bmatrix} e^{i\theta(s)/\epsilon}. \tag{2.3}$$

In (2.3) $\delta_m(\epsilon)$, $m = 0, 1, 2, \ldots$ with $\delta_0 = 1$, are the gauge functions of the asymptotic expansion. These functions are to be determined later by the process of matching inner and outer solutions. It turns out that δ_1 is equal to $\epsilon \ln \epsilon$ and δ_2 is equal to ϵ. For convenience, we will denote

$$\frac{d\theta(s)}{ds} = \alpha(s), \tag{2.4}$$

which is the complex wavenumber.

Substitution of (2.3) into (2.2) and upon partitioning terms according to $\delta_m(\epsilon)$, $m = 0, 1, 2, \ldots$, it is straightforward to find that the general mth-order equations can be cast into the form

$$\frac{\partial \hat{p}_m}{\partial r} - i\bar{\rho}(\omega - \alpha\bar{u})\hat{v}_m = R_m, \tag{2.5a}$$

$$\frac{\partial \hat{v}_m}{\partial r} - \frac{i}{\bar{\rho}(\omega - \alpha\bar{u})}\left[\bar{\rho}M^2(\omega - \alpha\bar{u})^2 - \frac{n^2}{r^2} - \alpha^2\right]\hat{p}_m + \left[\frac{1}{r} + \frac{\alpha}{\omega - \alpha\bar{u}}\frac{\partial \bar{u}}{\partial r}\right]\hat{v}_m = Q_m. \tag{2.5b}$$

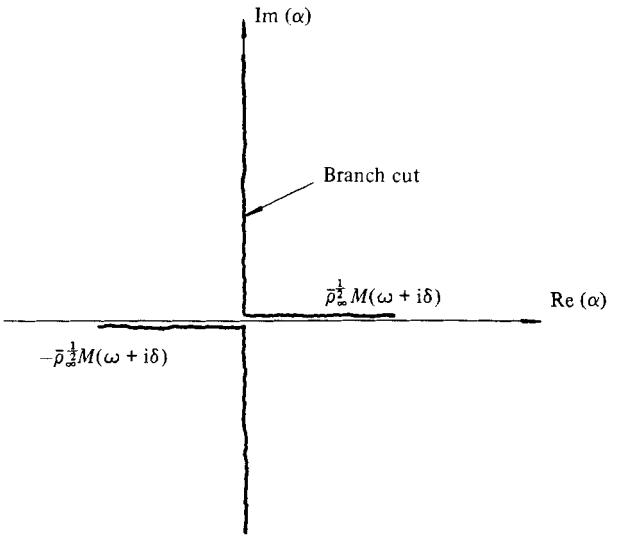

FIGURE 2. Branch cuts in the α-plane (limit $\delta \to 0^+$).

The nonhomogeneous terms R_m and Q_m in (2.5) depend on the lower-order solutions only. In particular, R_0, Q_0, R_1 and Q_1 are all equal to zero, so that the corresponding equations are homogeneous.

For $r > r_m$, on account of the mean flow (2.1), the equations for $\hat{p}_0$ and $\hat{v}_0$ become

$$\frac{\partial \hat{p}_0}{\partial r} - i\bar{\rho}_\infty \omega \hat{v}_0 = 0, \tag{2.6a}$$

$$\frac{\partial \hat{v}_0}{\partial r} - \frac{i}{\bar{\rho}_\infty \omega}\left(\bar{\rho}_\infty M^2\omega^2 - \frac{n^2}{r^2} - \alpha^2\right)\hat{p}_0 + \frac{\hat{v}_0}{r} = 0, \tag{2.6b}$$

where $\bar{\rho}_\infty$ is the dimensionless ambient density. Two linearly independent solutions of (2.6) are

$$\begin{bmatrix}\hat{p}_0\\ \hat{v}_0\end{bmatrix} = \begin{bmatrix} H_n^{(1)}(i\lambda r) \\ \dfrac{-i}{\bar{\rho}_\infty \omega}\dfrac{\partial}{\partial r} H_n^{(1)}(i\lambda r)\end{bmatrix}, \quad \begin{bmatrix}\hat{p}_0\\ \hat{v}_0\end{bmatrix} = \begin{bmatrix} H_n^{(2)}(i\lambda r) \\ \dfrac{-i}{\bar{\rho}_\infty \omega}\dfrac{\partial}{\partial r} H_n^{(2)}(i\lambda r)\end{bmatrix}. \tag{2.7a, b}$$

Here $H_n^{(1)}(\,)$ and $H_n^{(2)}(\,)$ are the nth-order Hankel functions of the first and second kind, and

$$\lambda(\alpha) = (\alpha^2 - \bar{\rho}_\infty M^2\omega^2)^{\frac{1}{2}}. \tag{2.8}$$

To facilitate the process of matching, branch cuts of λ are chosen such that $-\frac{1}{2}\pi \leqslant \arg[\lambda(\alpha)] < \frac{1}{2}\pi$ in the entire α-plane. This is shown in figure 2.

Let

$$\begin{bmatrix}\zeta_1^p\\ \zeta_1^v\end{bmatrix} \quad \text{and} \quad \begin{bmatrix}\zeta_2^p\\ \zeta_2^v\end{bmatrix}$$

be two linearly independent solutions of (2.5) for $m = 0$ such that for $r > r_m$ they are identically equal to the two solutions of (2.7). In terms of these functions the zeroth-order or the one-term inner solution may be expressed as

$$\begin{bmatrix}\hat{p}_0\\ \hat{v}_0\end{bmatrix} = A_0(s)\begin{bmatrix}\zeta_1^p(r,s)\\ \zeta_1^v(r,s)\end{bmatrix} + B_0(s)\begin{bmatrix}\zeta_2^p(r,s)\\ \zeta_2^v(r,s)\end{bmatrix}. \tag{2.9}$$

In (2.9) the amplitude functions $A_0(s)$ and $B_0(s)$ are arbitrary at this stage. The only constraint on this solution is that it must satisfy the finiteness condition at $r = 0$. That is, the functions

$$\lim_{r\to 0}\left\{A_0(s)\begin{bmatrix}\zeta_1^p(r,s)\\ \zeta_1^v(r,s)\end{bmatrix}+B_0(s)\begin{bmatrix}\zeta_2^p(r,s)\\ \zeta_2^v(r,s)\end{bmatrix}\right\} \quad \text{are bounded.} \tag{2.10}$$

3. The outer solution

The outer solution of (2.2) which describes the acoustic near and far field is to be valid in the region $r > r_m$. The appropriate outer variables are $(\bar{r}, s)$ (see Part 1), where $\bar{r} = \epsilon r$. In terms of these outer variables, (2.2), for small ϵ, becomes

$$\left.\begin{aligned}
-\mathrm{i}\frac{\omega}{\epsilon}v+\frac{\epsilon^2\bar{v}_\infty}{\bar{r}}\frac{\partial v}{\partial\bar{r}}+\epsilon^2 v\frac{\partial}{\partial\bar{r}}\left(\frac{\bar{v}_\infty}{\bar{r}}\right)&=-\frac{1}{\bar{\rho}_\infty}\frac{\partial p}{\partial\bar{r}},\\
-\mathrm{i}\frac{\omega}{\epsilon}w+\frac{\epsilon^2\bar{v}_\infty}{\bar{r}}\frac{\partial w}{\partial\bar{r}}+\epsilon^2\frac{\bar{v}_\infty w}{\bar{r}^2}&=-\frac{\mathrm{i}n}{\bar{\rho}_\infty\bar{r}}p,\\
-\mathrm{i}\frac{\omega}{\epsilon}u+\frac{\epsilon^2\bar{v}_\infty}{\bar{r}}\frac{\partial u}{\partial\bar{r}}&=-\frac{1}{\bar{\rho}_\infty}\frac{\partial p}{\partial s},\\
-\mathrm{i}\frac{\omega}{\epsilon}p+\frac{\epsilon^2\bar{v}_\infty}{\bar{r}}\frac{\partial p}{\partial\bar{r}}+\frac{1}{M^2}\left(\frac{1}{\bar{r}}\frac{\partial v\bar{r}}{\partial\bar{r}}+\frac{\mathrm{i}n}{\bar{r}}w+\frac{\partial u}{\partial s}\right)&=0.
\end{aligned}\right\} \tag{3.1}$$

A general solution of (3.1) satisfying the boundedness or radiation condition for large $\bar{r}$ may be constructed by first applying a Fourier transform to the variable s. Then by eliminating all other dependent variables in favour of $\tilde{u}$, the transform of u, it is straightforward to find that the equation to be solved is

$$\left(1-\frac{\epsilon^4\bar{\rho}_\infty M^2\bar{v}_\infty^2}{\bar{r}^2}\right)\frac{\partial^2\tilde{u}}{\partial\bar{r}^2}+\left(1+2\epsilon\mathrm{i}\bar{\rho}_\infty M^2\omega\bar{v}_\infty+\frac{\epsilon^4\bar{\rho}_\infty M^2\bar{v}_\infty^2}{\bar{r}^2}\right)\frac{1}{\bar{r}}\frac{\partial\tilde{u}}{\partial\bar{r}}$$
$$-\left(k^2-\frac{\bar{\rho}_\infty M^2\omega^2}{\epsilon^2}+\frac{n^2}{\bar{r}^2}\right)\tilde{u}=0, \tag{3.2}$$

where k is the Fourier transform variable. In Appendix A, it is shown how an exact solution of (3.2) satisfying the outgoing wave or boundedness condition as $\bar{r}\to\infty$ can be found in terms of a Hankel function of complex order for the axisymmetric wave mode ($n = 0$). For the higher-order wave modes, a similar solution valid to order ϵ^2 for all $\bar{r} > O(\epsilon^{1-1/N})$, where N is a large positive number, can also be found. By means of this solution the outer solution to order ϵ^2 may be written as an inverse Fourier transform as follows. Here only the expression for the pressure p will be given explicitly:

$$p^{\mathrm{O}}(\bar{r},s)=\int_{-\infty}^{\infty}g(k,\epsilon)\left(1+\frac{\mathrm{i}\epsilon^3\bar{v}_\infty}{\omega\bar{r}}\frac{\partial}{\partial\bar{r}}\right)[(\bar{r}^2-\epsilon^4\bar{\rho}_\infty M^2\bar{v}_\infty^2)^{-\frac{1}{2}\mathrm{i}\epsilon\bar{\rho}_\infty M^2\omega\bar{v}_\infty}$$
$$\times H_\nu^{(1)}(\mathrm{i}(\epsilon^2k^2-\bar{\rho}_\infty M^2\omega^2)^{\frac{1}{2}}(\bar{r}^2-\epsilon^4\bar{\rho}_\infty M^2\bar{v}_\infty^2)^{\frac{1}{2}}/\epsilon)]\,\mathrm{e}^{\mathrm{i}ks}\,\mathrm{d}k, \tag{3.3}$$

where $\nu=(n^2-\epsilon^2\bar{\rho}_\infty^2\omega^2M^4\bar{v}_\infty^2)^{\frac{1}{2}}$ and

$$g(k,\epsilon)=\frac{1}{2\pi}\int_{-\infty}^{\infty}\tilde{A}(s,\epsilon)\,\mathrm{e}^{\mathrm{i}\theta(s)/\epsilon-\mathrm{i}ks}\,\mathrm{d}s. \tag{3.4}$$

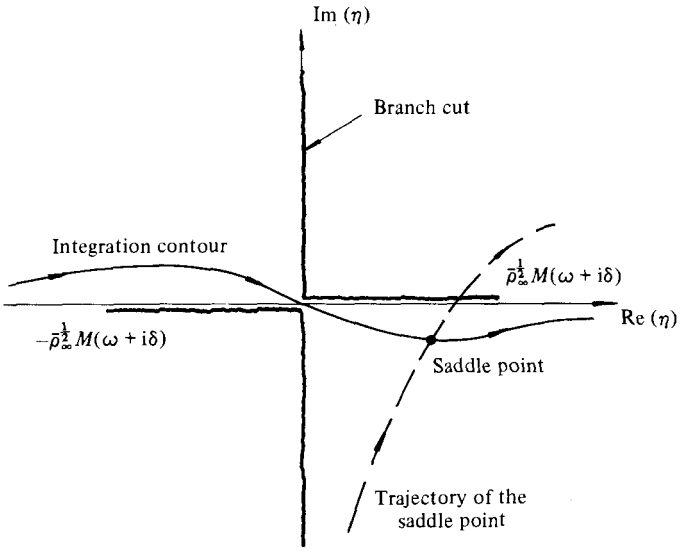

FIGURE 3. Branch cuts, saddle-point trajectory and integration contour in the complex η-plane.

In (3.3) $H_\nu^{(1)}(\ )$ is the νth-order Hankel function of the first kind. To ensure that the boundary condition at $\bar{r} \to \infty$ is satisfied, the branch cuts of the square-root function $\lambda(\eta) = (\eta^2 - \bar{\rho}_\infty M^2\omega^2)^{\frac{1}{2}}$, where $\eta = \epsilon k$, in the argument of the Hankel function will be taken such that $-\frac{1}{2}\pi \leqslant \arg[\lambda(\eta)] < \frac{1}{2}\pi$ in the entire complex η-plane. The actual configuration of the branch cuts is shown in figure 3. The amplitude function $\bar{A}(s, \epsilon)$ in (3.4) is arbitrary at this time. It will be determined by the matching process to be carried out in §4.

4. Matching of solutions

We will now follow the steps of Part 1 and match the solutions according to the intermediate matching principle of Van Dyke (1975) and Cole (1968). The appropriate intermediate variables (see Part 1) are $(\tilde{r}, s)$, where

$$\tilde{r} = \epsilon^{1/N} r. \tag{4.1}$$

For convenience, N in (4.1) will be taken as a large positive number. In the case of the axisymmetric instability-wave mode ($n = 0$), (3.3) and (3.4) give the exact outer solution to all powers of ϵ as $\epsilon \to 0$. Thus they also represent the intermediate solution. For the higher-order wave modes it can readily be shown that the intermediate solution to order ϵ^2 for $\tilde{r} \geqslant O(1)$ is the same as that given by (3.3) and (3.4) if a change of variable from $\bar{r}$ to $\epsilon^{1-1/N}\tilde{r}$ is made. Thus to order ϵ^2 with $\tilde{r}$ and s fixed the intermediate solution is

$$p(\tilde{r}, s) = \int_{-\infty}^{\infty} \frac{1}{\epsilon} g\left(\frac{\eta}{\epsilon}, \epsilon\right)\left(1 + \frac{i\epsilon^{1+2/N}\bar{v}_\infty}{\omega\tilde{r}} \frac{\partial}{\partial \tilde{r}}\right)[(\epsilon^{2-2/N}\tilde{r}^2 - \epsilon^4 \bar{\rho}_\infty M^2 \bar{v}_\infty^2)^{-\frac{1}{2}i\epsilon\bar{\rho}_\infty M^2\omega\bar{v}_\infty}$$
$$\times H_\nu^{(1)}(i\lambda(\eta)\,(\epsilon^{-2/N}\tilde{r}^2 - \epsilon^2\bar{\rho}_\infty M^2\bar{v}_\infty^2)^{\frac{1}{2}})]\, e^{i\eta s/\epsilon}\, d\eta, \tag{4.2}$$

where

$$\nu = (n^2 - \epsilon^2\bar{\rho}_\infty^2\,\omega^2 M^4 \bar{v}_\infty^2)^{\frac{1}{2}} \quad \text{and} \quad g\left(\frac{\eta}{\epsilon}, \epsilon\right) = \frac{1}{2\pi}\int_{-\infty}^{\infty} \bar{A}(s, \epsilon)\, e^{i(\theta(s) - \eta s)/\epsilon}\, ds. \tag{4.3}$$

In writing down (4.2) and (4.3) from (3.3) and (3.4), in addition to the change of variable from $\tilde{r}$ ro $\tilde{r}$, a change of integration variable from k to $\eta = \epsilon k$ has also been made. We will at this time expand the as yet unknown amplitude function $\tilde{A}(s,\epsilon)$ as an asymptotic series in the form

$$\tilde{A}(s,\epsilon) = \tilde{A}_0(s) + \epsilon\tilde{A}_1(s) + o(\epsilon). \tag{4.4}$$

Now with η fixed the integral of (4.3) may be evaluated asymptotically in the limit $\epsilon \to 0$ by the saddle-point method (see Dingle 1973). This yields, as in Part 1, an asymptotic expansion of $g(\eta/\epsilon,\epsilon)$. On substituting this asymptotic expansion into (4.2) and keeping the intermediate variables s and $\tilde{r}$ fixed, the integral on the right-hand side may again be evaluated by the saddle-point method. This gives the intermediate limit of the outer solution. To order ϵ the asymptotic expansion, denoted by a superscript o, is

$$\begin{aligned}\lim_{\epsilon\to 0} p^{o}(\tilde{r},s) \underset{\tilde{r},\,s\,\text{fixed}}{\sim} e^{i\theta(s)/\epsilon}\Big\{&\tilde{A}_0(s)\,[1-(\epsilon\ln\epsilon)\,i\bar{\rho}_\infty M^2\omega\bar{v}_\infty]\,H_n^{(1)}(i\lambda\epsilon^{-1/N}\tilde{r})\\ &+\epsilon\Big[(\tfrac{1}{2}\pi\bar{\rho}_\infty M^2\omega\bar{v}_\infty\tilde{A}_0\delta_{n0}+\tilde{A}_1+E(\epsilon^{-1/N}\tilde{r}))\,H_n^{(1)}(i\lambda\epsilon^{-1/N}\tilde{r})\\ &\qquad+F(\epsilon^{-1/N}\tilde{r})\frac{\partial}{\partial(\epsilon^{-1/N}\tilde{r})}H_n^{(1)}(i\lambda\epsilon^{-1/N}\tilde{r})\Big]+O(\epsilon^2\ln\epsilon)\Big\},\end{aligned} \tag{4.5}$$

where

$$E(\epsilon^{-1/N}\tilde{r}) = -i\bar{\rho}_\infty M^2\omega\bar{v}_\infty\tilde{A}_0\ln(\epsilon^{-1/N}\tilde{r}) - \frac{i\alpha^2\alpha'\tilde{A}_0}{2\lambda^4}((\lambda\epsilon^{-1/N}\tilde{r})^2+n^2),$$

$$F = \frac{i\bar{v}_\infty\tilde{A}_0}{\omega\epsilon^{-1/N}\tilde{r}} + \frac{i}{2\lambda^4}(\bar{\rho}_\infty M^2\omega^2\alpha'\tilde{A}_0 - 2\lambda^2\alpha\tilde{A}_0' + \alpha^2\alpha'\tilde{A}_0)\,\epsilon^{-1/N}\tilde{r},$$

$$\lambda = (\alpha^2-\bar{\rho}_\infty M^2\omega^2)^{\frac{1}{2}},\quad \alpha' = \frac{d\alpha(s)}{ds},\quad \tilde{A}_0' = \frac{d\tilde{A}_0(s)}{ds},$$

$$\delta_{n0} = \begin{cases}1 & (n=0),\\ 0 & \text{otherwise.}\end{cases}$$

The one-term inner solution is given by (2.9) and (2.3). The intermediate limit of this solution, designated by a superscript i, is

$$\lim_{\epsilon\to 0} p^{i}(\tilde{r},s) \underset{\tilde{r},\,s\,\text{fixed}}{\sim} e^{i\theta(s)/\epsilon}[A_0(s)\,H_n^{(1)}(i\lambda\epsilon^{-1/N}\tilde{r}) + B_0(s)\,H_n^{(2)}(i\lambda\epsilon^{-1/N}\tilde{r})]. \tag{4.6}$$

On comparing (4.5) and (4.6) it is easy to verify that matching of solutions in the intermediate limit to order unity requires

$$A_0(s) = \tilde{A}_0(s) \tag{4.7}$$

and

$$B_0(s) = 0. \tag{4.8}$$

Now with $B_0 = 0$ the boundedness condition of (2.10) will, in general, not be satisfied unless the remaining unknown function $\alpha(s)$ takes on special values. In other words, the one-term inner solution is an eigenvalue problem with α as an eigenvalue. As in Part 1 we will only consider the eigenvalue corresponding to an instability wave of the jet flow.

To match the solutions to higher order it is noted that the next two higher-order terms in (4.5) are of order $\epsilon\ln\epsilon$ and ϵ respectively. This suggests that the gauge functions $\delta_1(\epsilon)$ and $\delta_2(\epsilon)$ of the inner expansion (2.3) should be chosen as

$$\delta_1(\epsilon) = \epsilon\ln\epsilon,\quad \delta_2(\epsilon) = \epsilon. \tag{4.9}$$

With this choice of δ_1 the equations for $\hat{p}_1$ and $\hat{v}_1$ as given by (2.5) are identical with those for $\hat{p}_0$ and $\hat{v}_0$. Thus $(\hat{p}_1, \hat{v}_1)$ must have the same form of solution as $(\hat{p}_0, \hat{v}_0)$. In order that the inner solution, to order $\epsilon \ln \epsilon$, matches that of (4.5) in the intermediate limit, it is straightforward to verify that the appropriate inner solution for $(\hat{p}_1, \hat{v}_1)$ is

$$\begin{bmatrix} \hat{p}_1(r,s) \\ \hat{v}_1(r,s) \end{bmatrix} = -\mathrm{i}\bar{\rho}_\infty M^2 \omega \bar{v}_\infty A_0 \begin{bmatrix} \zeta_1^p(r,s) \\ \zeta_1^v(r,s) \end{bmatrix}. \tag{4.10}$$

The governing equations for $(\hat{p}_2, \hat{v}_2)$, the ϵ-order term, of the inner solution, are (2.5a, b) with $m = 2$. These equations are non-homogeneous. The non-homogeneous terms R_2 and Q_2 are linear functions of A_0 and A_0'. If these non-homogeneous equations are considered as a system of first-order differential equations, the solution can readily be constructed by means of the method of fundamental matrix (see Boyce & DiPrima 1977, chap. 7). The fundamental matrix $\boldsymbol{\Psi}$ and its inverse $\boldsymbol{\Psi}^{-1}$ are

$$\boldsymbol{\Psi}(r,s) = \begin{pmatrix} \zeta_1^p & \zeta_2^p \\ \zeta_1^v & \zeta_2^v \end{pmatrix}, \quad \boldsymbol{\Psi}^{-1} = \frac{1}{W(\zeta_1, \zeta_2)} \begin{pmatrix} \zeta_2^v & -\zeta_2^p \\ -\zeta_1^v & \zeta_1^p \end{pmatrix}, \tag{4.11}$$

where $W(\zeta_1, \zeta_2)$ is the Wronskian. In the present problem it is easy to show that W is given by

$$W(\zeta_1, \zeta_2) = -\frac{4(\omega - \alpha\bar{u})}{\pi \bar{\rho}_\infty \omega^2 r}. \tag{4.12}$$

In terms of $\boldsymbol{\Psi}$ and $\boldsymbol{\Psi}^{-1}$ the solution for $(\hat{p}_2, \hat{v}_2)$ may be written as

$$\begin{bmatrix} \hat{p}_2 \\ \hat{v}_2 \end{bmatrix} = A_1(s) \begin{bmatrix} \zeta_1^p \\ \zeta_1^v \end{bmatrix} + \boldsymbol{\Psi} \int_0^r \boldsymbol{\Psi}^{-1}(r', s) \begin{bmatrix} R_2(r', s) \\ Q_2(r', s) \end{bmatrix} \mathrm{d}r'. \tag{4.13}$$

For $r > r_\mathrm{m}$ the functions in $\boldsymbol{\Psi}^{-1}$, R_2 and Q_2 are expressible in terms of Hankel functions. Thus the integrand of (4.13) involves products of Hankel functions and powers of r'. It turns out that they can all be integrated in closed forms using formulas provided by Watson (1966) and Gradshteyn & Ryzhik (1965). By means of this explicit order-ϵ inner solution, the intermediate limit of the three-term inner solution can be determined in a straightforward manner. Up to order ϵ the intermediate limit of the inner solution is

$$\begin{aligned} \lim_{\epsilon \to 0} p^{\mathrm{i}}(\tilde{r}, s) \underset{\tilde{r},\, s \text{ fixed}}{\sim} \mathrm{e}^{\mathrm{i}\theta(s)/\epsilon} \Big\{ & A_0 [1 - (\epsilon \ln \epsilon)\, \mathrm{i}\bar{\rho}_\infty M^2 \omega \bar{v}_\infty] H_n^{(1)}(\mathrm{i}\lambda \epsilon^{-1/N} \tilde{r}) \\ & + \epsilon \Big[((\bar{E} + E(\epsilon^{-1/N}\tilde{r}))\, H_n^{(1)}(\mathrm{i}\lambda \epsilon^{-1/N}\tilde{r}) \\ & + F(\epsilon^{-1/N}\tilde{r}) \frac{\partial}{\partial(\epsilon^{-1/N}\tilde{r})} H_n^{(1)}(\mathrm{i}\lambda \epsilon^{-1/N}\tilde{r}) + D H_n^{(2)}(\mathrm{i}\lambda \epsilon^{-1/N}\tilde{r}) \Big] \Big\}, \end{aligned} \tag{4.14}$$

where

$$\begin{aligned} \bar{E} = A_1 - \frac{\pi \bar{\rho}_\infty \omega^2}{4} \Big[\int_0^{r_\mathrm{m}} \frac{r}{\omega - \alpha\bar{u}} (\zeta_2^v R_2 - \zeta_2^p Q_2)\, \mathrm{d}r + \int_{r_\mathrm{m}} \frac{r}{\omega} (\zeta_2^v R_2 - \zeta_2^p Q_2)\, \mathrm{d}r \Big] \\ - \frac{\mathrm{i}n(2\alpha A_0' + \alpha' A_0)}{2\lambda^2} + \frac{2\mathrm{i}\alpha^2 \alpha' A_0 (n^2 + 2n)}{4\lambda^4}, \end{aligned}$$

$$D = -\frac{\pi \bar{\rho}_\infty \omega^2}{4} \Big[\int_0^{r_\mathrm{m}} \frac{r}{\omega - \alpha\bar{u}} (\zeta_1^p Q_2 - \zeta_1^v R_2)\, \mathrm{d}r + \int_{r_\mathrm{m}} \frac{r}{\omega} (\zeta_1^p Q_2 - \zeta_1^v R_2)\, \mathrm{d}r \Big].$$

By comparing (4.14) and (4.5) it is clear that matching of solutions to terms of order ϵ requires

$$\bar{E} = \tfrac{1}{2}\pi\bar{\rho}_\infty M^2\omega\bar{v}_\infty \tilde{A}_0\,\delta_{n0} + \tilde{A}_1, \tag{4.15}$$

and

$$D = 0. \tag{4.16}$$

Condition (4.15) relates $\tilde{A}_1$ to A_1 and A_0. Condition (4.16) when written out in full gives the equation

$$I_1(s)\frac{\mathrm{d}A_0}{\mathrm{d}s} + I_2(s)\,A_0 = 0. \tag{4.17}$$

The full expressions for $I_1(s)$ and $I_2(s)$ are given in Appendix B. Equation (4.17) is the amplitude equation for $A_0(s)$, which after one integration yields the solution

$$A_0(s) = \hat{A}_0 \exp\left[-\int_0^s \frac{I_2}{I_1}\,\mathrm{d}s\right]. \tag{4.18}$$

With $A_0(s)$ determined by (4.18), the complete solution of the instability wave and its associated sound field of a supersonic axisymmetric jet to the lowest order is found. Numerical results of this solution (both the inner and the outer solution) will be compared with experimental measurements in §6.

5. The near pressure field and the directivity of sound in the far field

In the region outside the jet flow, i.e. $r > r_{\mathrm{m}}$, the near-field solution associated with the instability wave of the nth azimuthal mode of the jet is given by equations (3.3) and (3.4) of the outer solution. To the lowest order, the formula for the near pressure field may be simplified to

$$p(r, x, \phi, t) = \int_{-\infty}^{\infty} g(\eta)\, H_n^{(1)}(\mathrm{i}\lambda(\eta)\, r)\, \mathrm{e}^{\mathrm{i}(\eta x + n\phi - \omega t)}\,\mathrm{d}\eta, \tag{5.1}$$

$$g(\eta) = \frac{1}{2\pi}\int_{-\infty}^{\infty} A_0(\epsilon x)\, \mathrm{e}^{\mathrm{i}\theta(\epsilon x)/\epsilon - \mathrm{i}\eta x}\,\mathrm{d}x, \tag{5.2}$$

where $\lambda(\eta) = (\eta^2 - \bar{\rho}_\infty M^2\omega^2)^{\frac{1}{2}}$. By means of (5.1) it is easy to find that the root-mean-square intensity of pressure fluctuations associated with an instability wave in the near field is equal to

$$(\bar{p}^2)^{\frac{1}{2}} = \frac{1}{\sqrt{2}}\left|\int_{-\infty}^{\infty} g(\eta)\, H_n^{(1)}(\mathrm{i}\lambda r)\, \mathrm{e}^{\mathrm{i}(\eta x + n\phi)}\,\mathrm{d}\eta\right|. \tag{5.3}$$

Not all the near-field pressure fluctuations are radiated into the far field as sound. To find the power of sound emitted, it is advantageous to use a spherical coordinate system (R, χ, θ) centred at the nozzle exit of the jet with the polar axis aligned in the direction of flow. These spherical coordinates are related to the cylindrical coordinates (x, r, ϕ) by

$$x = R\cos\chi, \quad r = R\sin\chi. \tag{5.4}$$

In terms of R, χ and ϕ (5.1) becomes

$$p(R, \chi, \phi, t) = \int_{-\infty}^{\infty} g(\eta)\, H_n^{(1)}(\mathrm{i}\lambda(\eta)\, R\sin\chi)\, \mathrm{e}^{\mathrm{i}\eta\cos\chi R + \mathrm{i}n\phi - \mathrm{i}\omega t}\,\mathrm{d}\eta. \tag{5.5}$$

For large R the Hankel function may be replaced by its asymptotic form. This gives

$$p(R, \chi, \phi, t) \underset{R\to\infty}{=} \int_{-\infty}^{\infty} \frac{g(\eta)\exp\{\mathrm{i}[\mathrm{i}\lambda(\eta)\sin\chi + \eta\cos\chi]R + \mathrm{i}n\phi - \mathrm{i}\omega t - \frac{1}{2}\mathrm{i}n\pi - \frac{1}{4}\mathrm{i}\pi\}}{(\frac{1}{2}\pi\mathrm{i}\lambda(\eta)\, R\sin\chi)^{\frac{1}{2}}}\,\mathrm{d}\eta. \tag{5.6}$$

Now the integral on the right-hand side of (5.6) can be evaluated by the method of stationary phase (see Tam & Morris 1980). The stationary-phase point in this case is located at $\eta = \bar{\rho}_\infty^{\frac{1}{2}} M\omega \cos\chi$ in the η-plane. On carrying out the stationary-phase integration we obtain

$$p(R,\chi,\phi,t) \underset{R\to\infty}{=} \frac{2}{R} g(\bar{\rho}_\infty^{\frac{1}{2}} M\omega\cos\chi)\exp\left[\mathrm{i}(\bar{\rho}_\infty^{\frac{1}{2}} M\omega R + n\phi - \omega t) - \tfrac{1}{2}\mathrm{i}(n+1)\pi\right]. \quad (5.7)$$

Finally, from (5.7) the following formula for the sound power $D(\chi)$ radiated in direction χ per unit solid angle by an excited instability wave (see Tam 1975) may be derived:

$$D(\chi) = \lim_{R\to\infty} \tfrac{1}{2}R^2|p|^2 = 2|g(\bar{\rho}_\infty^{\frac{1}{2}} M\omega\cos\chi)|^2. \quad (5.8)$$

6. Numerical results and comparison with experiment

In this section numerical results of the inner and outer solutions corresponding to the excited instability waves and their associated noise fields of a cold, nearly perfectly expanded axisymmetric supersonic jet of Mach number 2.1 will be presented. These theoretical results will then be compared with the experimental measurements of Troutt (1978) and Troutt & McLaughlin (1982). In the present calculation the measured mean-velocity profiles under excitation will be used in determining the propagation characteristics of the instability waves. As discussed before, this is a relatively simple way of accounting for the effects of nonlinear interaction between the excited instability waves and the mean flow. Mean-flow data of Troutt's experiment at a forcing frequency corresponding to a Strouhal number $St = 0.2$ have been reported by McLaughlin, Seiner & Liu (1980) and Troutt & McLaughlin (1982). For convenience the jet will be divided into three regions. In each region the measured mean-flow profiles will be approximated by simple analytical functions. These regions are the core, the transition and the developed regions as shown in figure 1. In the core region, the mean flow is uniform in the central part of the jet. Surrounding this uniform core is a mixing layer with a velocity profile which can be approximated closely by a half-Gaussian function, as has been demonstrated by Troutt & McLaughlin (1982). On taking these facts into consideration, the mean velocity in this part of the jet will be approximated by

$$\bar{u} = \begin{cases} 1 & (r < h), \\ \exp\left[-(\ln 2)\left(\dfrac{r-h(x)}{b(x)}\right)^2\right] & (h \leqslant r). \end{cases} \quad (6.1)$$

In (6.1) $h(x)$ is the radius of the uniform core and $b(x)$ is the half-width of the annular mixing layer, i.e. the radial distance from the outer edge of the uniform core to the half-velocity point as shown in figure 4. The axial distribution of $b(x)$ measured by Troutt taken from McLaughlin *et al.* (1980) interpolated by a cubic spline curve will be used. The core region extends over the first five diameters of the jet. Within this region of the jet the same set of data by Troutt reveals that $h(x)$ and $b(x)$ are related in such a way that the total axial momentum flux of the jet is practically a constant. This property of momentum-flux conservation is well known in most free shear flow. Here it will be employed to provide a continuous axial distribution of h in the subsequent calculation.

The developed region of Troutt's Mach-number 2.1 jet begins at about eight diameters downstream of the nozzle exit. In this region the mean flow evolves

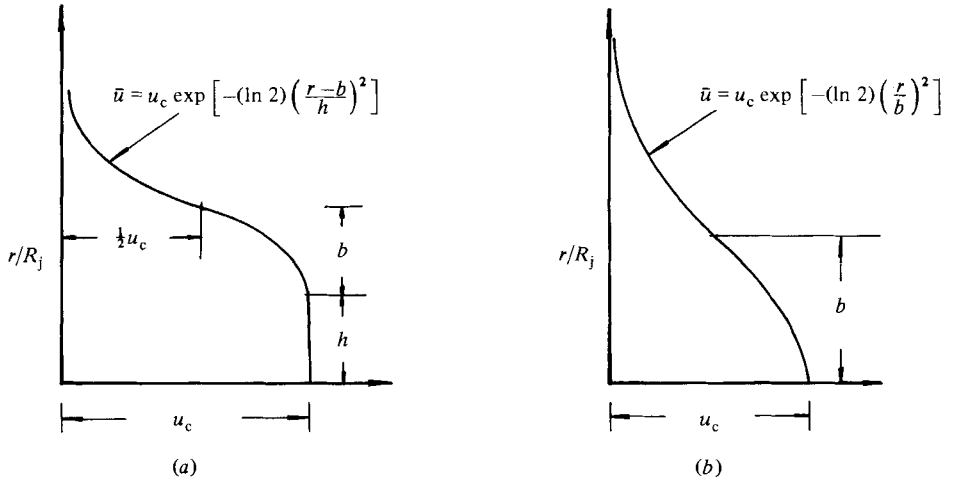

FIGURE 4. Axial mean-velocity profile in (*a*) the core ($u_c = 1$) and the transition regions, and (*b*) the developed region of the jet.

gradually into a self-similarity form. To a good approximation this form may be analytically represented by a two-parameter Gaussian function:

$$\bar{u} = u_c(x) \exp\left[-(\ln 2)\left(\frac{r}{b(x)}\right)^2\right], \tag{6.2}$$

where $u_c(x)$ is the centreline velocity of the jet and $b(x)$ is the half-width of the velocity profile. In this region the principle of conservation of axial momentum flux is again applicable. Once more it will be used to relate the two parameters $u_c(x)$ and $b(x)$. This relationship has been tested against the measurements of Troutt. Very favourable agreement (see figure 6) is found. As in the core region, Troutt's measured values of $b(x)$ interpolated by a cubic spline curve will be used as an input to the computation of the mean-flow velocity given by (6.2).

The transition region is where the mean flow of the jet changes smoothly from the core flow to a fully developed similarity flow. In this region the form of the mean velocity profile should match smoothly to those of (6.1) and (6.2) at the beginning and the end of the transition region respectively. Here the following mean-axial-velocity profile containing three parameters will be used:

$$\bar{u} = \begin{cases} u_c(x) & (r < h), \\ u_c(x) \exp\left[-(\ln 2)\left(\dfrac{r-h(x)}{b(x)}\right)^2\right] & (h \leqslant r). \end{cases} \tag{6.3}$$

It is easy to show if the values of the three parameters u_c, b and h are chosen appropriately, (6.3) can readily be made to satisfy the smooth-joining requirement. To provide further smoothness in the overall mean-velocity profile the x-dependences of the three parameters $u_c(x)$, $b(x)$ and $h(x)$ are assumed to be in the form of a cubic spline. The coefficients of the spline curve are chosen such that, at where the velocity profiles (6.1)–(6.3) are joined together, not only the parameters u_c, b and h are continuous but their first derivatives in x are also continuous. This degree of smoothness is needed to guarantee a genuine slowly varying mean flow as required by the theory.

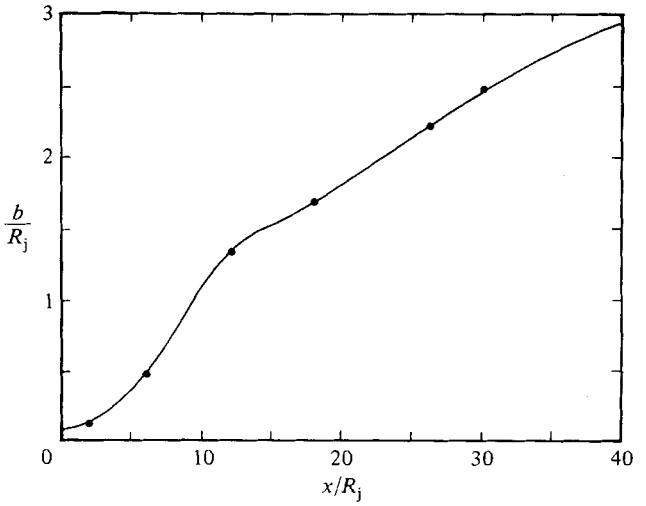

FIGURE 5. Axial distribution of mean-velocity profile parameter for an excited ($St = 0.2$) Mach-number 2.1 supersonic jet: ●, Troutt's measurements from McLaughlin *et al.* (1980); ——, spline curve fit.

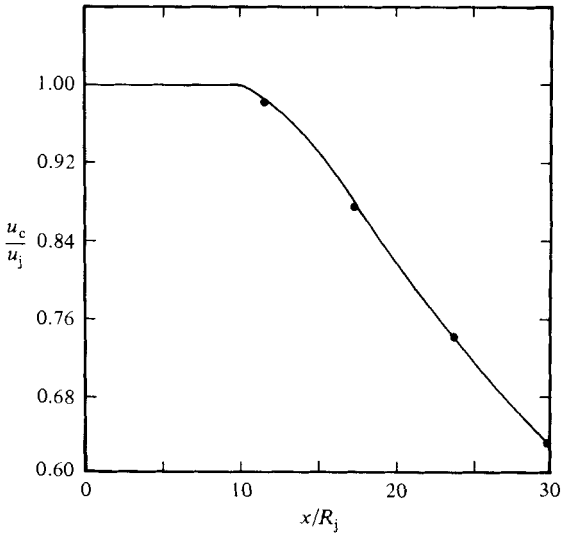

FIGURE 6. Axial distribution of mean centreline velocity for an excited ($St = 0.2$) Mach-number 2.1 supersonic jet: ●, Troutt (1978); ——, from conservation of momentum flux.

Away from the jet, say at $r > h+3b$, the mean axial velocity is negligibly small and has no dynamical significance as far as noise generation by instability waves is concerned. Therefore in the numerical computation $\bar{u}$ will be taken to be zero outside the region $r = h+3b$ (i.e. $r_m = h+3b$) along the entire length of the jet. Figure 5 shows the empirically fitted axial distribution of b over the first twenty diameters of the jet based on the measured data of Troutt (see McLaughlin *et al.* 1980). The corresponding distribution of centreline velocity u_c of the three empirical velocity profiles (6.1)–(6.3) as determined by the principle of conservation of momentum flux and spline curve fit is shown in figure 6. As can be seen, the calculated value of u_c agrees favourably with the measurements of Troutt (1978) over most of the noise-producing region of the jet.

6.1. *Calculation of instability waves and comparison with experiment*

To compute the spatial distribution of the physical variables associated with an instability wave of a fixed Strouhal and mode number, the first step is to calculate the local eigenvalue or the complex wavenumber $\alpha(s)$. Mathematically the eigenvalue problem for $\alpha(s)$ consists of finding a solution (ζ_1^p, ζ_1^v) to (2.5), which for $r > r_m$ is identically equal to (2.7*a*) and remains bounded as $r \to 0$. Numerically the simplest way to solve this eigenvalue problem is to integrate (2.5) over the range $r = 0$ to $r = r_m$ in two parts. The first part of the numerical integration starts at r_m using (2.7) as the starting value. The integration is to be performed in the direction towards the jet axis and continued until a value of r, say $r = \mathrm{Re}\,(r_c)$, near the critical point of the differential equation (r_c is given by $\omega - \alpha\bar{u}(r_c) = 0$) is reached. The second part of the numerical integration starts at a point very close to $r = 0$. Here the starting solution can be determined by solving equation (2.5) using the method of Frobenius series. For the problem under consideration it can be shown that only one of the series solutions expanded about $r = 0$ is bounded at $r = 0$. The bounded solution is the correct solution to initiate the integration near the jet axis. On reaching the point $r = \mathrm{Re}\,(r_c)$ two sets of values for (ζ_1^p, ζ_1^v) are now available. They are, however, unequal unless the value of α used in the calculation is an eigenvalue. In other words, if we form the difference of these two solutions α is the root of this difference function. The root of this difference function can now be found iteratively by a variety of standard numerical techniques (e.g. Newton's iteration method). In the present numerical computation, the iteration procedure is allowed to continue until the estimated error of the calculated eigenvalue is no more than half a percent. One-half of a percent is the upper error bound in all our numerical calculations. We believe this should be adequate for comparison with experimental measurements.

In the region sufficiently far downstream from the jet exit the excited wave would no longer grow in amplitude. Instead, it is damped. For damped waves two modifications are needed in implementing the above numerical integration scheme. First of all, the present model assumes an inviscid fluid. As has been discussed by Tam & Morris (1980), the correct solution for inviscid damped waves is to be obtained by analytic continuation of that of the unstable wave in the complex r-plane. The integration contour must be deformed around the critical point $r = r_c$. This can be carried out easily by using a rectangular deformed contour (see Tam 1975; Tam & Morris 1980). For the Mach-number 2.1 supersonic jet under consideration, the phase velocities of the instability waves (at $St = 0.2$ and 0.4) are supersonic relative to the ambient speed of sound. This is true even when these waves reach the damped region of the jet. They are therefore 'damped supersonic waves'. Hence, in accordance with §7 of Part 1, the value of α in the second Riemann sheet of the complex α-plane should be used to evaluate the value of $\lambda(\alpha)$ in the starting condition of (2.7). With these modifications the numerical procedure for the determination of the local eigenvalue α as described above can again be carried out.

After the complex wavenumber α of a fixed value of x is determined numerically to an acceptable degree of accuracy, the eigenfunction is computed. The eigenfunction is used to evaluate the two integrals I_1 and I_2 of (4.18). The full analytical expressions of these integrals are given in Appendix B. For damped waves these integrals are to be integrated over the same deformed contour used to determine the eigenvalue α and the eigenfunction (see Tam & Morris 1980). The above steps of computation are repeated for a preselected set of appropriately spaced values of x. These calculated values of I_2/I_1 are then used to determine numerically the integral and the

exponential factor of (4.18). In this way the spatial distribution of the amplitude function A_0 for a given wave mode and Strouhal number, save for a multiplicative constant $\hat{A}_0$, is known. Here the spatial variation of A_0 provides the non-parallel-flow correction, both in amplitude and in phase, for the instability-wave solution.

In the experiment of Troutt (1978) and Troutt & McLaughlin (1982) instability waves were excited by a single point glow discharge mounted flush near the nozzle exit. This method of excitation is incapable of producing individual azimuthal wave modes. Instead a combination of several instability-wave modes are generated. The measurements of Troutt & McLaughlin show, however, that the excited motion of the jet is dominated by the contributions of the three lowest-order unstable azimuthal wave modes. They are the axisymmetric mode ($n = 0$) and the left- and right-hand helical modes ($n = \pm 1$). To separate these modes, near-field microphone measurements on a circle of radius equal to three jet diameters were taken. The centre of the circle is located on the jet axis and is twelve jet diameters downstream of the nozzle exit. These measurements permit Troutt and McLaughlin to determine the relative amplitudes and phases of the waves in their jet. This information is used in the present calculation to calculate the relative values of the unknown initial complex amplitudes $\hat{A}_0$ of the three excited instability waves. By linearly combining the three waves with the corresponding relative initial amplitudes and phases, the excited instability wave motion at any point in the jet is found except for one remaining unknown multiplicative constant.

As has been noted above, three dominant modes of instability waves are generated when a jet is excited by a point glow discharge. Because of the phase differences between the axisymmetric ($n = 0$) and the flapping modes ($n = \pm 1$) the resulting motion of the jet is asymmetric in the two halves of the plane containing the axis of the jet and the point glow discharge. In the experiment of Troutt and McLaughlin all the measurements were taken in the half-plane on the same side as the point glow discharge. In comparing the present calculation with their experimental measurements the numerical results on this same half-plane will be used. Figure 7 shows the calculated axial distribution of centreline mass velocity fluctuation $(\overline{pu})_{\mathrm{rms}}$ at an excitation Strouhal number of 0.4. Also plotted in this figure are the measurements of Troutt & McLaughlin (1982). These measurements are, however, not given in absolute magnitude but are non-dimensionalized with respect to the measured value at one point. That is to say, only the relative distribution of the centreline mass velocity distribution is available for comparison with calculation. Therefore in figure 7, for the purpose of comparing theory and experiment, the unknown multiplicative constant of the calculated distribution of mass-velocity fluctuation has been chosen such that the peak value is the same as that of the measurements. As can be seen, there is good general agreement between the calculated and the measured results. The calculated curve peaks at nearly the same location as the measured data. In addition, the decay part of the calculated root-mean-squared mass-velocity distribution matches very well with Troutt's experimental observations. Figure 8 shows a similar comparison between the calculated and the measured results at a Strouhal number of 0.2. Again there is good qualitative agreement in general. However, unlike the Strouhal-number 0.4 case the agreement is not as good. As can be seen in this figure, the computed curve peaks about four jet radii upstream of the measured data points. It implies that the noise source of the calculated results is located somewhat upstream of the measured data. This difference should be borne in mind when comparing the calculated and the measured near pressure field later on. At the present time it is not possible to determine the exact cause of this difference. There are several

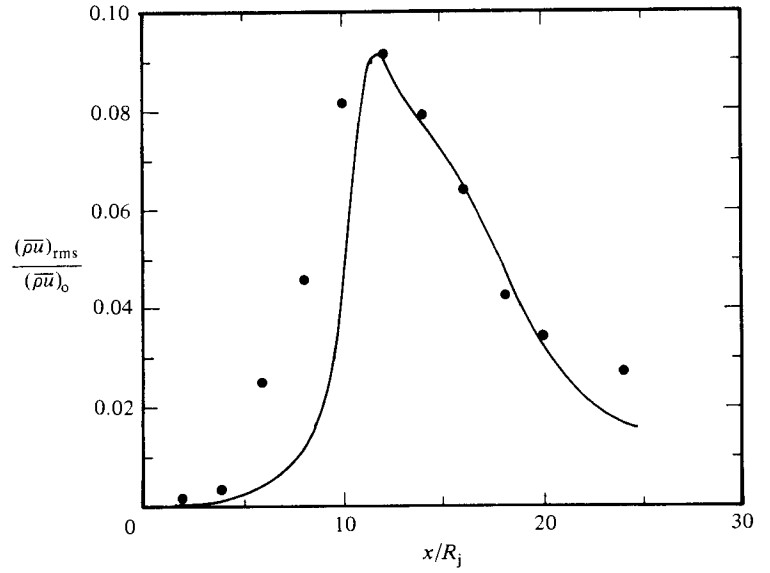

FIGURE 7. Comparison of measured (●, Troutt & McLaughlin 1982) and calculated (——) axial distribution of centreline mass-velocity fluctuation of a Mach-number 2.1 jet excited at $St = 0.4$.

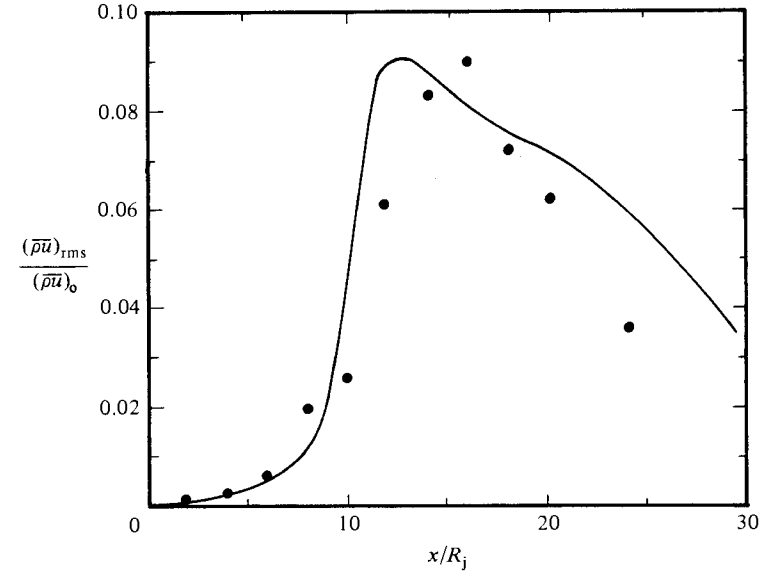

FIGURE 8. Comparison of measured (●, Troutt & McLaughlin 1982) and calculated (——) axial distribution of centreline mass velocity fluctuation of a Mach-number 2.1 jet excited at $St = 0.2$.

possibilities. As no experimental error estimates are provided by Troutt & McLaughlin (1982), it becomes difficult to judge which possibility is more likely. Despite this difference, the overall agreement between observations and predictions appears to be reasonably good. This is especially true in view of the fact that the calculation is practically free from any adjustable parameter.

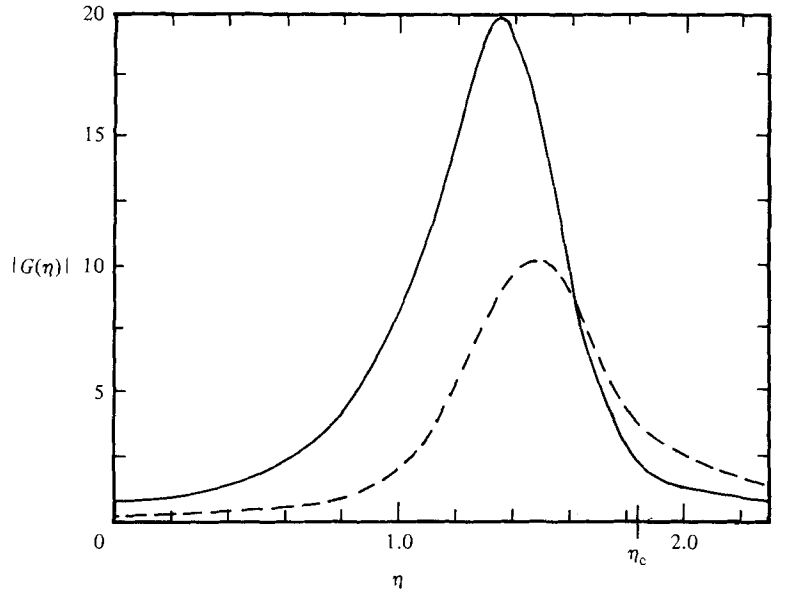

FIGURE 9. Calculated wavenumber spectrum $|G(\eta)|$ for $St = 0.4$: ——, mode $n = 0$; - - - - -, mode $n = 1$.

6.2. *Near-field pressure-level contours and comparison with experiment*

The near pressure field associated with an instability wave of the nth mode is given by (5.1) and (5.2). In (5.2) the amplitude function A_0 and phase function θ are the same as those of the excited instability wave. They are, except for a multiplicative constant, completely determined. To compute the near-field pressure contours, the integral of (5.2) is first evaluated by the method of fast Fourier transform (FFT) (see e.g. Cooley, Lewis & Welch 1967, 1969; Brigham 1974). The transform function $g(\eta)$ gives the complex-wavenumber spectrum of the pressure fluctuations in the near and far field. Figures 9 and 10 show the calculated wavenumber spectra of the excited jet at Strouhal numbers 0.4 and 0.2 for the $n = 0$ and $n = 1$ modes. The point η_c ($\eta_c = \bar{\rho}_\infty^{\frac{1}{2}} M\omega$) in these figures is the branch point of the function $\lambda(\eta)$ of figure 3. The physical significance of this point is that wave components to the left of this point propagate with supersonic phase velocities relative to the ambient sound speed, while those on the right have subsonic phase velocities. Of all these wave components only those wave components with supersonic phase velocity radiate into the far field. The direction of radiation of each wave component is given by (5.8). As can be seen in figures 9 and 10, the wave spectrum of each mode is dominated by a peak located in the supersonic region. This indicates that a sizeable fraction of the pressure disturbances in the near field would radiate into the far field as sound. Moreover, it infers that the near-field pressure-level contours and the far-field directivity are highly directional. These are the characteristics of supersonic jet noise.

To compute the near-field pressure-level contours (contours of constant root-mean-squared pressure fluctuations) the Fourier integral of (5.1) is evaluated numerically again by means of the method of fast Fourier transform. For a given radial distance r the fast Fourier transform generates a set of values of p at regular intervals of x. To cover the entire near field it is therefore necessary to repeat the FFT calculation over a set of regularly spaced values of r. In this way, values of the

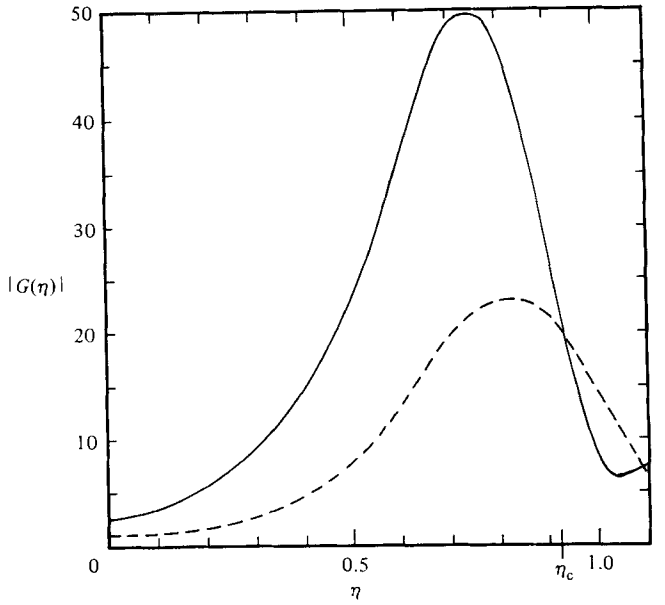

FIGURE 10. Calculated wavenumber spectrum $|G(\eta)|$ for $St = 0.2$: ——, mode $n = 0$; - - - - -, mode $n = 1$.

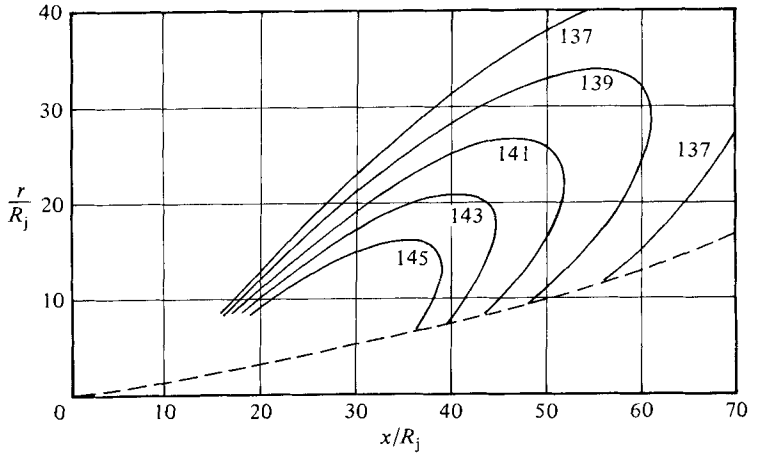

FIGURE 11. Calculated near-field sound-pressure-level contours associated with an instability wave of $St = 0.2$, mode $n = 0$ (SPL dB Re 2×10^{-5} N/m^2).

complex pressure function p at a set of rectangular grid points covering the near field are determined. Contours of constant pressure amplitudes can then be constructed by interpolation between the grid points. In the present calculation this step was carried out by a computer subprogram. Figure 11 illustrates the calculated near-field pressure-level contours associated with the $St = 0.2$, mode $n = 0$ instability wave of the jet. The magnitudes of the contours are labelled in decibel (dB re 2×10^{-5} N/m^2). The lobed appearance of this figure indicates strong noise radiation in a direction at approximately 40° from the jet axis. Figure 12 shows a similar plot of the calculated near-field pressure-level contours for the $n = 1$ mode at the same Strouhal number. In this case the lobed characteristic of the contours is not as apparent. This means that

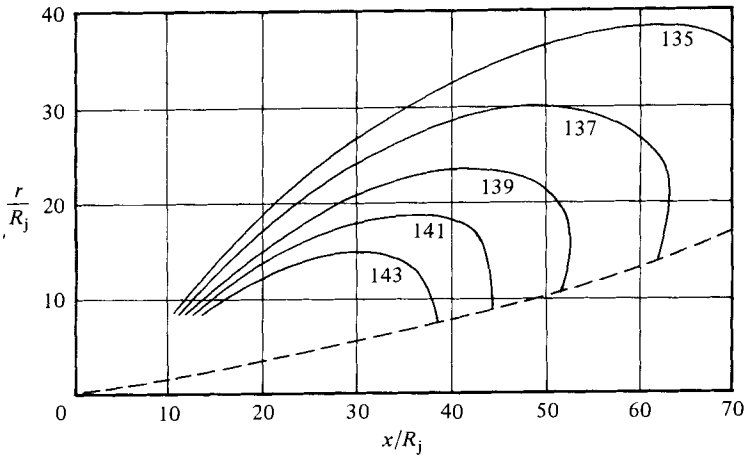

FIGURE 12. Calculated near-field sound-pressure-level contours associated with an instability wave of $St = 0.2$, mode $n = 1$ (SPL dB Re 2×10^{-5} N/m^2).

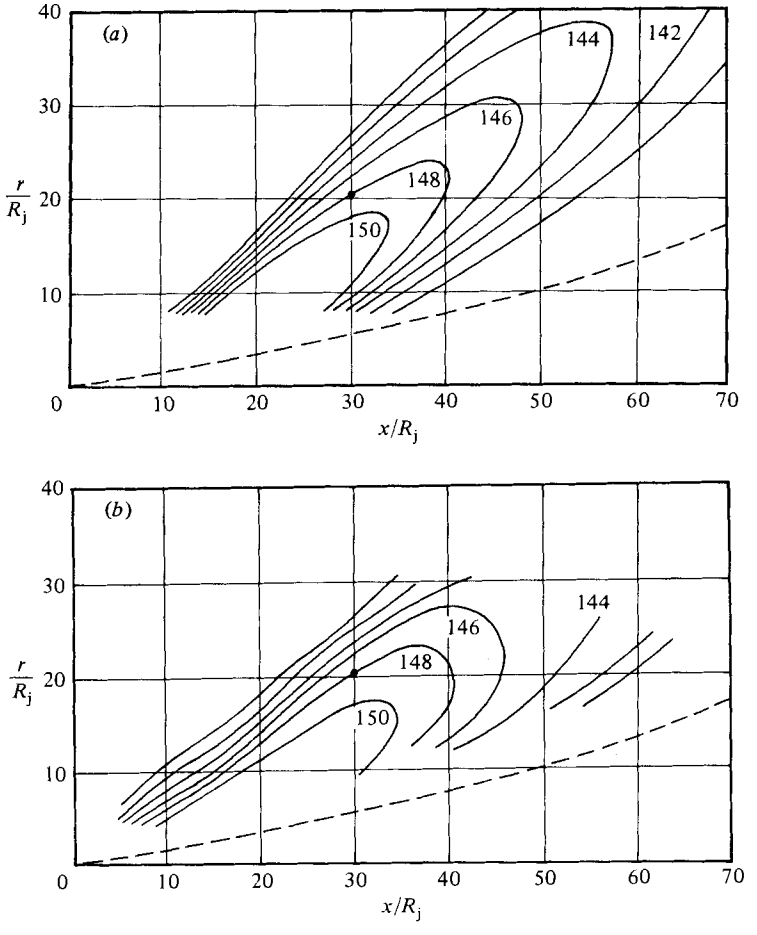

FIGURE 13. Near-field sound-pressure-level contours for jet excited at $St = 0.4$: (*a*) calculated; (*b*) measured (Troutt & McLaughlin 1982) (SPL dB Re 2×10^{-5} N/m^2).

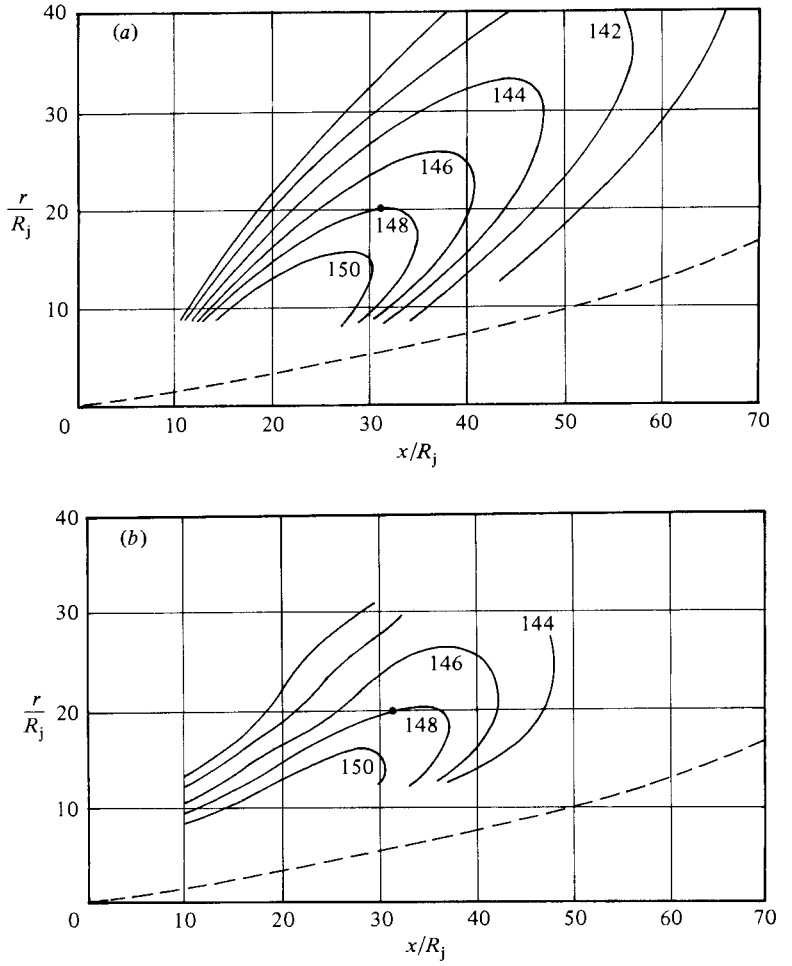

FIGURE 14. Near-field sound-pressure-level contours for jet excited at $St = 0.2$: (*a*) calculated; (*b*) measured (Troutt & McLaughlin 1982) (SPL dB Re 2×10^{-5} N/m^2).

sound would be radiated with more or less uniform intensity by this instability-wave mode over most of the angles lying within a cone of 35° measured from the jet axis.

In the experiment of Troutt & McLaughlin (1982) three dominant instability wave modes are excited simultaneously. Therefore, to compare the calculated results with experimental measurements the complex pressure function of (5.1) for the three modes are added together (the relative phases of these waves are important to the final results) and the sum is used to determine the pressure contour field. Figure 13 (*a*) shows the calculated near-field pressure-level contours of the jet excited at a Strouhal number of 0.4. The corresponding experimental measurements obtained by Troutt (1978) and Troutt & McLaughlin (1982) is given in figure 13 (*b*). Since the calculated results have an unknown multiplicative constant, the absolute pressure level cannot be predicted. In figure 13 (*a*) the magnitude of the constant is chosen so that the calculated pressure level at the point marked by a black circle is 148 dB, the same as the corresponding point in figure 13 (*b*). On comparing these two figures it is clear that there is excellent agreement. The agreement between the calculated and the measured

150 dB and 148 dB contours is nearly perfect. The lobed nature of the contours, the direction of the lobe and the spacings of the contours are correctly predicted. Figures 14(*a*, *b*) show a similar comparison between the calculated and the measured near-field pressure level contours at a Strouhal number of 0.2. As pointed out in §6.1, the calculated instability wave peaks upstream of the measured data. This implies that the field shape of the calculated near pressure field would be displaced upstream relative to Troutt and McLaughlin's observations. To compare with the measurements shown in figure 14(*b*) the entire calculated near field of figure 14(*a*) has been moved about four jet diameters downstream. Again the absolute intensity of the pressure is adjusted as before so that the pressure level at the point marked by a black circle is 148 dB matching the value of the corresponding point in figure 14(*b*). With this adjustment, which reflects solely the discrepancy in calculating the instability waves at this Strouhal number, there is again excellent agreement between the calculated results and measurements. The direction of peak sound radiation as defined by the lobe of the calculated contours and that of the measurements are practically the same. The field shape and the relative spacings of the contours of the two figures are again in almost total agreement.

All in all, it seems reasonable to conclude that very favourable agreements between theoretical calculations based on the method of matched asymptotic expansions and experimental measurements are found. The compared results include the predicted instability-wave amplitude distribution using the inner solution and the near-field pressure-level contours using the outer solution. These very favourable agreements strongly suggest that the method of solution developed in the Part 1 paper is indeed valid. Furthermore, they also offer concrete support to the proposition made previously by a number of investigators that instability waves are important noise sources of supersonic jets (at least, for those of low to moderately high Reynolds numbers).

7. Concluding remarks

In this paper the method of solution developed in Part 1 (Tam & Burton 1984) is applied to the study of instability waves and their associated sound field of axisymmetric supersonic jets. To test the validity of the theory, the calculated results of a Mach-number 2.1 cold supersonic jet are compared with the experimental measurements of Troutt (1978) and Troutt & McLaughlin (1982). Two series of comparisons at excitation Strouhal numbers 0.4 and 0.2 have been carried out. Very favourable agreements are found both in the calculated instability-wave amplitude distribution (the inner solution) and the near pressure field level contours (the outer solution) in each case. These very favourable comparisons with measurements (which have not been obtained before in jet-noise research) clearly indicate that the physical model used and the method of solution developed are valid.

In closing it is worthwhile to point out that the method developed in this and in Part 1 for predicting the near pressure field of a jet is somewhat unique. At the present time there is no other known method in the literature that allows one to calculate the unsteady near pressure field of supersonic jets. To be able to predict the far-field noise of a jet requires merely a moderately accurate model of the noise sources inside the jet. This is because only a fraction of the fluctuating pressure components associated with the unsteady motion of the jet radiates into the far field. In the near field, however, both the non-propagating hydrodynamic components as well as the radiated sound are important. Hence to predict the near field both of these

components must be calculated correctly. This in turn requires a correct modelling and solution of the unsteady components of the flow. From this standpoint it is therefore not surprising that near-field sound-pressure prediction has not been very successful before.

This work was supported by the National Aeronautics and Space Administration under grant NAG 3-182.

Appendix A

In this appendix the solution of (3.2) is discussed. The relationships between $\tilde{u}$ and the other dependent variables are

$$\tilde{v} = \frac{1}{ik}\frac{\partial \tilde{u}}{\partial \bar{r}}, \quad \tilde{w} = \frac{n}{k\bar{r}}\tilde{u}, \quad \tilde{p} = \frac{\bar{\rho}_\infty}{k}\left[\frac{\omega}{\epsilon}\tilde{u} + i\epsilon^2 \frac{\bar{v}_\infty}{\bar{r}}\frac{\partial \tilde{u}}{\partial \bar{r}}\right]. \tag{A 1}$$

Let $y = \bar{r}^2 - \epsilon^4 \bar{\rho}_\infty M^2 \bar{v}_\infty^2$ be a new independent variable, then (3.2) becomes

$$\frac{\partial^2 \tilde{u}}{\partial y^2} + \frac{1 + i\epsilon\bar{\rho}_\infty M^2 \omega \bar{v}_\infty}{y}\frac{\partial \tilde{u}}{\partial y} - \left[\frac{k^2 - \bar{\rho}_\infty(\omega/\epsilon)^2 M^2}{4y} + \frac{n^2}{4y^2}\right]\tilde{u} = -\frac{n^2\epsilon^4 \bar{\rho}_\infty M^2 \bar{v}_\infty^2 \tilde{u}}{4y^2(y + \epsilon^4 \bar{\rho}_\infty M^2 \bar{v}_\infty^2)}. \tag{A 2}$$

For the axisymmetric wave mode ($n = 0$) the right-hand side of (A 2) is identically equal to zero. For the higher-order modes it is straightforward to show that the term on the right-hand side is of order ϵ^2 compared with the term $n^2\tilde{u}/4y^2$ on the left-hand side of the equation for $y \geqslant O(\epsilon^{2-1/N})$. Upon neglecting this order-ϵ^2 term, it is easy to find that the solution of (A 2) may be expressed in terms of a Hankel function of complex argument as

$$\tilde{u} = y^{-\frac{1}{2}i\epsilon\bar{\rho}_\infty M^2 \omega \bar{v}_\infty} H_\nu^{(1)}(i(k^2\epsilon^2 - \bar{\rho}_\infty \omega^2 M^2)^{\frac{1}{2}} y^{\frac{1}{2}}/\epsilon), \tag{A 3}$$

where $\nu = (n^2 - \epsilon^2 \bar{\rho}_\infty^2 M^4 \omega^2 \bar{v}_\infty^2)^{\frac{1}{2}}$. Note that this solution is exact in the case of the axisymmetric ($n = 0$) instability-wave mode.

Appendix B

The functions I_1 and I_2 of (4.17) are

$$I_1 = \frac{\alpha r_m^2}{\bar{\rho}_\infty \omega}[(H_n^{(1)}(i\lambda r_m))^2 - H_{n+1}^{(1)}(i\lambda r_m) H_{n-1}^{(1)}(i\lambda r_m)] + \int_0^{r_m} \frac{\omega r}{\hat{\omega}}\left[\bar{\rho}\bar{u}(\zeta_1^v)^2 - M^2\bar{u}(\zeta_1^p)^2 - \frac{\omega}{\hat{\omega}}\zeta_1^p \zeta_1^u - \frac{n\bar{u}}{\hat{\omega}r}\zeta_1^p \zeta_1^w - \frac{\alpha}{\bar{\rho}\hat{\omega}}(\zeta_1^p)^2\right] dr,$$

$$I_2 = \frac{\bar{v}_\infty}{\bar{\rho}_\infty \omega^2}\left[\frac{\partial}{\partial r}H_n^{(1)}(i\lambda r_m)\right]^2 + M^2\bar{v}_\infty [H_n^{(1)}(i\lambda r_m)]^2 + \frac{\alpha' r_m^2}{2\bar{\rho}_\infty \omega}\left[(H_n^{(1)}(i\lambda r_m))^2 - H_{n+1}^{(1)}(i\lambda r_m) H_{n-1}^{(1)}(i\lambda r_m)\right] + \frac{\alpha\alpha'\lambda' r_m^2}{\bar{\rho}_\infty \omega\lambda} H_{n+1}^{(1)}(i\lambda r_m) H_{n-1}^{(1)}(i\lambda r_m)$$

$$+ \int_0^{r_m} \frac{\omega r}{\hat{\omega}}\left[\bar{\rho}\bar{v}_1 \zeta_1^v \frac{\partial \zeta_1^v}{\partial r} + \bar{\rho}(\zeta_1^v)^2 \frac{\partial \bar{v}_1}{\partial r} + \bar{\rho}\bar{u}\zeta_1^v \frac{\partial \zeta_1^v}{\partial s} - M^2\bar{v}_1 \zeta_1^p \frac{\partial \zeta_1^p}{\partial r}\right.$$

$$- M^2\bar{u}\zeta_1^p \frac{\partial \zeta_1^p}{\partial s} - \frac{\omega}{\hat{\omega}}\zeta_1^p \frac{\partial \zeta_1^u}{\partial s} - \frac{n\bar{v}_1}{\hat{\omega}r}\zeta_1^p \frac{\partial \zeta_1^w}{\partial r} - \frac{n\bar{v}_1}{\hat{\omega}r^2}\zeta_1^p \zeta_1^w$$

$$\left. - \frac{n\bar{u}}{\hat{\omega}r}\zeta_1^p \frac{\partial \zeta_1^w}{\partial s} - \frac{\alpha\bar{v}_1}{\hat{\omega}}\zeta_1^p \frac{\partial \zeta_1^u}{\partial r} - \frac{\alpha}{\hat{\omega}}\frac{\partial \bar{u}}{\partial s}\zeta_1^p \zeta_1^u - \frac{\alpha}{\bar{\rho}\hat{\omega}}\zeta_1^p \frac{\partial \zeta_1^p}{\partial s}\right] dr,$$

where $\hat{\omega} = \omega - \alpha\bar{u}$.

REFERENCES

BOYCE, W. E. & DIPRIMA, R. C. 1977 *Elementary Differential Equations.* Wiley.

BRIGHAM, E. O. 1974 *The Fast Fourier Transform.* Prentice-Hall.

CHAN, Y. Y. & WESTLEY, R. 1973 Directional acoustic radiation generated by spatial jet instability. *Can. Aero. and Space Inst. Trans.* **6**, 36–41.

COLE, J. D. 1968 *Perturbation Methods in Applied Mathematics.* Blaisdell.

COOLEY, J. W., LEWIS, P. A. & WELCH, P. D. 1967 Application of the fast Fourier transform to computation of Fourier integrals, Fourier series, and convolution integrals. *IEEE Trans. Audio and Electro Acoust.* **15**, 79–84.

COOLEY, J. W., LEWIS, P. A. & WELCH, P. D. 1969 The fast Fourier transform and its applications. *IEEE Trans. Education* **12**, 27–34.

DINGLE, R. B. 1973 *Asymptotic Expansions: Their Derivation and Interpretation.* Academic.

GRADSHTEYN, I. S. & RYZHIK, I. W. 1965 *Table of Integrals, Series and Products.* Academic.

MCLAUGHLIN, D. K., SEINER, J. M. & LIU, H. 1980 On the noise generated by large scale instabilities in supersonic jets. *AIAA Paper* 80-0964.

TAM, C. K. W. 1971 Directional acoustic radiation from a supersonic jet generated by shear layer instability. *J. Fluid Mech.* **46**, 757–768.

TAM, C. K. W. 1975 Supersonic jet noise generated by large-scale disturbances. *J. Sound Vib.* **38**, 51–79.

TAM, C. K. W. & MORRIS, P. J. 1980 The radiation of sound by the instability waves of a compressible plane turbulent shear layer. *J. Fluid Mech.* **98**, 349–381.

TAM, C. K. W. & BURTON, D. E. 1984 Sound generated by instability waves of supersonic flows. Part 1. Two-dimensional mixing layers. *J. Fluid Mech.* **138**, 249–271.

TROUTT, T. R. 1978 Measurements on the flow and acoustic properties of a moderate-Reynolds-number supersonic jet. Ph.D. thesis, Oklahoma State University.

TROUTT, T. R. & MCLAUGHLIN, D. K. 1982 Experiments on the flow and acoustic properties of a moderate Reynolds number supersonic jet. *J. Fluid Mech.* **116**, 123–156.

VAN DYKE, M. 1975 *Perturbation Methods in Fluid Mechanics.* Parabolic.

WATSON, G. N. 1966 *A Treatise on the Theory of Bessel Functions*, 2nd edn. Cambridge University Press.

WHITHAM, G. B. 1974 *Linear and Nonlinear Waves.* Wiley-Interscience.